Liu *et al. Energy Mater* 2022;2:200007
DOI: 10.20517/energymater.2022.03

Energy Materials

Communication

Open Access

Check for updates

Atomistic engineering of Ag/Pt nanoclusters for remarkably boosted mass electrocatalytic activity

Liangzhen Liu[1,#], Qiang-Yu Zhu[2,3,#], Junwei Li[1], Junxiang Chen[1], Junheng Huang[1], Qing-Fu Sun[2,*], Zhenhai Wen[1,*]

[1]CAS Key Laboratory of Design and Assembly of Functional Nanostructures, Fujian Provincial Key Laboratory of Nanomaterials, Fujian Institute of Research on the Structure of Matter, Chinese Academy of Sciences, Fuzhou 350002, Fujian, China.
[2]State Key Laboratory of Structural Chemistry, Fujian Institute of Research on the Structure of Matter, Chinese Academy of Sciences, Fuzhou 350002, Fujian, China.
[3]University of Chinese Academy of Science, Beijing 100049, China.
[#]Authors contributed equally.

***Correspondence to:** Prof. Zhenhai Wen, CAS Key Laboratory of Design and Assembly of Functional Nanostructures, Fujian Provincial Key Laboratory of Nanomaterials, Fujian Institute of Research on the Structure of Matter, Chinese Academy of Sciences, YangqiaoWest Street 155, Fuzhou 350002, Fujian, China. E-mail: wen@fjirsm.ac.cn; Prof. Qing-Fu Sun, State Key Laboratory of Structural Chemistry, Fujian Institute of Research on the Structure of Matter, Chinese Academy of Sciences, YangqiaoWest Street 155, Fujian 350002, Fuzhou, China. E-mail: qfsun@fjirsm.ac.cn

How to cite this article: Liu L, Zhu QY, Li J, Chen J, Huang J, Sun QF, Wen Z. Atomistic Engineering of Ag/Pt nanoclusters for remarkably boosted mass electrocatalytic activity. *Energy Mater* 2022;2:200007. https://dx.doi.org/10.20517/energymater.2022.03

Received: 20 Jan 2022 **First Decision:** 4 Feb 2022 **Revised:** 26 Feb 2022 **Accepted:** 7 Mar 2022 **Published:** 31 Mar 2022

Academic Editors: Yuping Wu, Hao Liu **Copy Editor:** Jia-Xin Zhang **Production Editor:** Jia-Xin Zhang

Abstract

It is of vital importance to boost the intrinsic activity and augment the active sites of expensive and scarce platinum-based catalysts for advancing a variety of electrochemical energy applications. We herein report a mild electrochemical bottom-up approach to deposit ultrafine, but stable, Pt_8Ag_4 alloy clusters on carbon nanotubes (CNTs) by elaborately designing bimetallic organic cluster precursors with four silver and eight platinum atoms coordinated with μ,σ-bridged ethynylpyridine ligands, i.e., $[Ag_4(C_{24}H_{16}N_4Pt)_8(BF_4)_4]$. The Pt_8Ag_4 cluster/CNT hybrids present impressively high platinum mass activity that is threefold that of commercial Pt/C toward the hydrogen evolution reaction, as a result of the cooperative contributions from the Ag atoms that enhance the intrinsic activity and the CNT supports that increase the activity sites. The present work affords an attractive avenue for engineering and stabilizing Pt-based nanoclusters at the atomic level and represents a promising strategy for the development of high-efficiency and durable electrocatalysts.

Keywords: Pt_8Ag_4 clusters, electrocatalyst, high mass electrocatalytic activity, hydrogen evolution reaction

INTRODUCTION

Platinum (Pt)-based materials are generally recognized as state-of-the-art catalysts that are indispensable for a variety of electrochemical energy conversion cells. Developing efficient and stable Pt-based catalysts with high intrinsic activity and exposed active sites is crucial for hydrogen and fuel cell technologies, as it is more commercially viable to minimize the loading content of expensive and scarce Pt. On this basis, at least two strategies have been proposed to promote the mass activity of Pt catalysts. One is to develop precisely atomically engineer Pt nanoparticles or sub-nanometer nanoclusters, because the unique features of ultrasmall nanoparticles or nanoclusters, including a high ratio of surface-to-bulk atoms, electronic and geo-metric shell closings and quantum confinement, endow them with a remarkably enhanced catalytic activity that cannot be obtained in bulk samples [1-6]. The other strategy is to tailor or alloy Pt with heterometal atoms, which may tune the electronic structure of Pt-based catalysts and thus feasibly promote its intrinsic activity and enhance the utilization efficiency of platinum metal[7-11]. In essence, an ideal electrocatalyst should have rich catalytic active sites, high intrinsic catalytic activity and long-term stability[12-14].

Recently, extensive efforts have been devoted to the controllable synthesis of metallic organic clusters (MOCs) because M_nL_m-type (M: Metal; n: Number of metal atoms; L: Ligand; m: Number of ligands) nanoclusters tend to present attractive physiochemical properties[15]. Although molecule-like bimetallic alloy nanoclusters represent a new type of catalysts that may bridge homogeneous and heterogeneous catalysis and potentially avoid the disadvantages of conventional pyrolysis alloys, the controllable synthesis of stable alloy nanoclusters remains a grand challenge that is yet to be resolved[16-20]. Moreover, tiny nanoclusters often suffer from poor structural integrity due to their easy aggregation and fusion during the synthesis and treatment processes, leading to a decreased density of active sites and poor catalytic durability and efficiency[19]. It is thus desirable to load these tiny nanoclusters on suitable support but the weak interaction between the metal atoms and supports often leads to metal sintering and deactivation upon catalysis operation. Another disadvantage that must be overcome is the poor conductivity of MOCs, which can also lead to poor electrochemical performance.

In this regard, we herein report the first synthesis of Pt_8Ag_4 bimetallic organic clusters (Pt_8Ag_4 MOCs) through the reaction between a Pt-based metalloligand and Ag^+, which can be evolved into alloyed Pt_8Ag_4 clusters through *in-situ* electrochemical decoration on the surface of carbon nanotubes (CNTs). This approach greatly improves the conduction of the catalyst and also can increase its stability during operation by increasing the interaction between the metal atoms and supports. Finally, the formation of the Pt_8Ag_4 cluster/CNT hybrids results in an enhanced mass electrocatalytic activity toward the hydrogen evolution reaction (HER) with mg-1 Pt at an overpotential of 70 mV.

RESULTS AND DISCUSSION

Scheme 1 shows the procedure for the synthesis of the bimetallic Pt_8Ag_4 clusters/CNTs. The Pt metalloligand was synthesized by standard Cu-catalyzed coupling reactions between the (bpy)$PtCl_2$ precursor (bpy = 2,2'-bipyridine) and 4-ethynylpyridine (≡ py) in the presence of triethylamine in dichloromethane at room temperature [Supplementary Scheme 1]. The Pt metalloligand has two pendant 4-pyridyl units, which can further coordinate with $AgBF_4$ to form the bimetallic organic clusters [$Ag_4(C_{24}H_{16}N_4Pt)_8(BF_4)_4$, Pt_8Ag_4 MOCs]. The Pt_8Ag_4 MOCs were then modified onto the CNT surface through the interaction of π-π stacking between MOCs and CNTs, which were finally evolved into Pt_8Ag_4 clusters/CNTs by an electrochemical

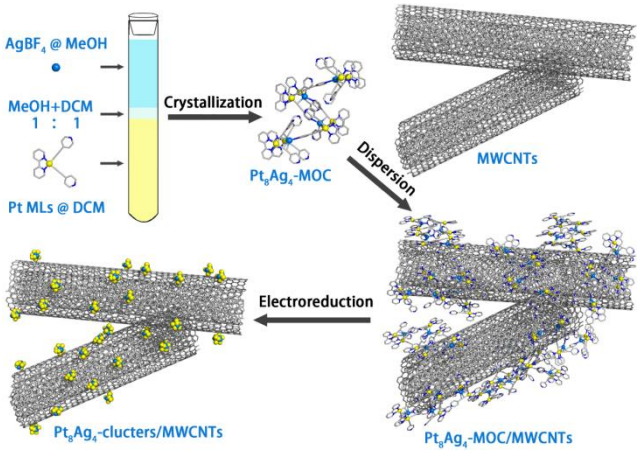

Scheme 1. Schematic diagram of the preparation of Pt_8Ag_4 clusters/CNTs. CNT: Carbon nanotubes.

reduction method. For comparison, Pt/CNTs were also prepared for comparison using Pt metalloligands as precursors with a similar process to the Pt_8Ag_4 clusters/CNTs.

The X-ray single-crystal structure of the Pt_8Ag_4-MOC precursor is shown in Figure 1A, which reveals a two-layered sandwich structure with a rhombic shape defined by four Pt_2Ag units, with diagonal lengths of 1.12 and 2.28 nm and a thickness of 0.39 nm (defined by the corresponding Pt to Pt distances). Each layer consists of four (bpy)Pt(≡ py)$_2$ metalloligands and four Ag ions, which are all sandwiched between two (bpy)Pt(≡ py)$_2$ ligands through multiple μ-coordination to the ethynyl groups and PtAgPt metallophilic interactions (with Pt-Ag distances of 2.86-3.42 Å). Interligand Ag-py coordination along with inter-layer π-π stacking interactions between the (bpy)Pt planes finally connect together with the unique discrete supramolecular architecture [Figure 1A, Supplementary Figure 1]. The powder X-ray diffraction (PXRD) patterns of the Pt_8Ag_4 MOCs present good agreement with the simulated PXRD pattern [Figure 1B], indicating the successful preparation of bimetallic organic cluster precursors. [Figure1C-D] display the high-resolution transmission electron microscopy (HRTEM) images of the Pt_8Ag_4 MOCs/CNTs, revealing that the MOCs are uniformly decorated on the CNT surface due to the interaction of π-π stacking between Pt_8Ag_4 MOCs and CNTs.

The Pt_8Ag_4 MOCs have a size range of 1.5-2.5 nm [inset of Figure 1D], consistent with the theoretical value of the Pt_8Ag_4 MOC crystal structures.[Figure 1E-F] exhibit the HRTEM images of the Pt_8Ag_4 cluster/CNT hybrids, from which one can observe that the Pt_8Ag_4 clusters, like Pt_8Ag_4 MOCs, are uniformly dispersed on CNTs with a size range of 1.5-3.5 nm, close to that of the Pt_8Ag_4 MOCs This indicates that the robust structure of the Pt_8Ag_4 MOCs can effectively prevent metal clusters from aggregation during the electrochemical reduction process. From the TEM images [Figure 1G], one can observe that the geometry of the Pt_8Ag_4 clusters is close to that of the rhombic crystal molecules and diffraction fringes with a d-spacing of 0.230 nm [inset of Figure 1G], corresponding to the (111) crystal plane of the face-centered cubic structure[21-23]. It is found that the d-spacing of the diffraction fringes in Pt_8Ag_4 are located in between the d-spacing of the crystal planes of Pt (0.226 nm) and Ag (0.235 nm)[24,25].

Based on the XRD pattern of the Pt_8Ag_4 clusters/CNTs, Pt/CNTs and Pt_8Ag_4 MOCs/CNTs [Supplementary Figure 2], one can clearly observe two broad peaks at ~26° and ~44° for all samples, corresponding to the characteristic crystal planes of CNTs[26]. There are no diffraction peaks corresponding to metallic Pt or Ag, likely due to the low Pt and/or Ag contents and their ultrasmall nanoclusters in the hybrids. Figure 1H-J

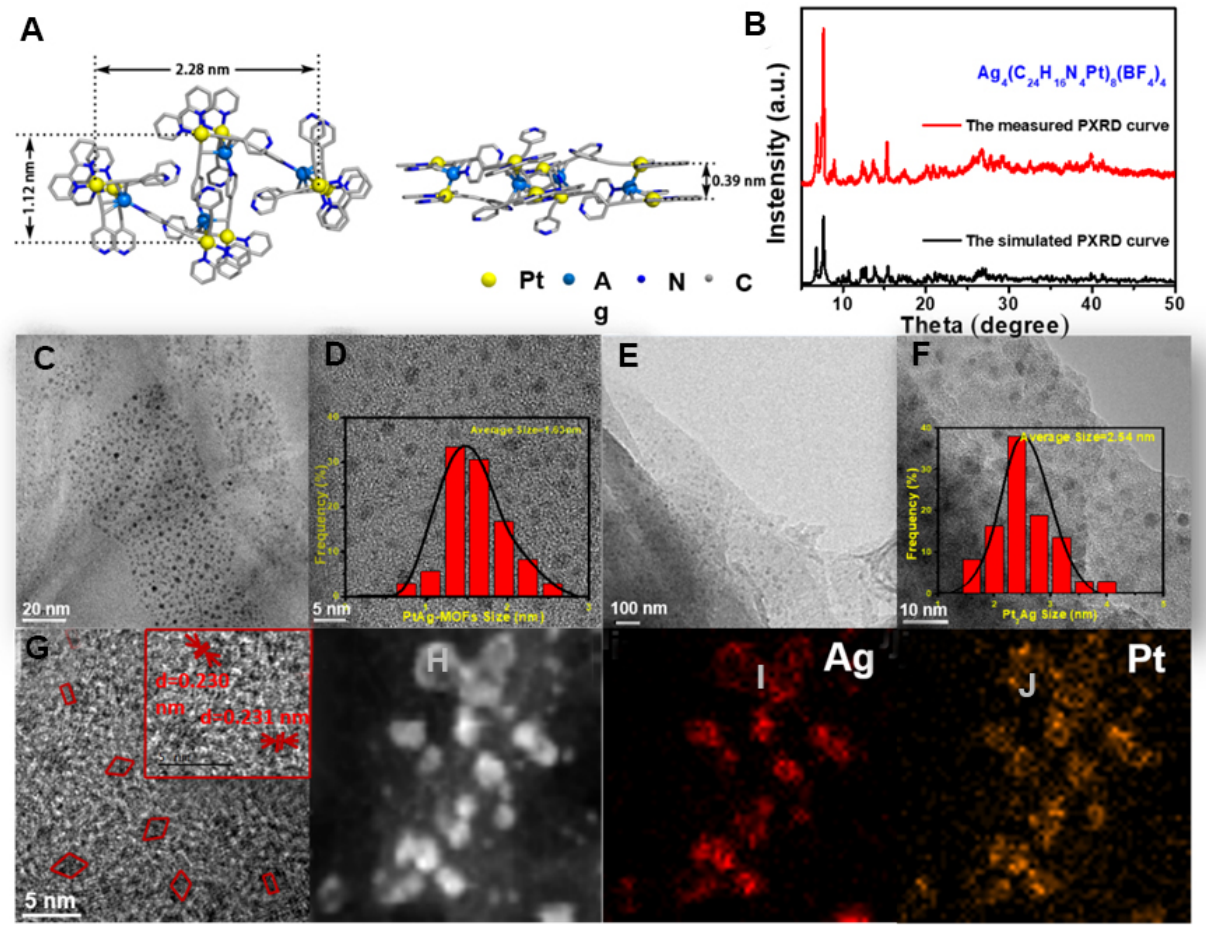

Figure 1. (A) Crystalline structure and (B) PXRD pattern of $Ag_4(C_{24}H_{16}N_4Pt)_8(BF_4)_4$. (C, D) HRTEM images of Pt_8Ag_4-MOCs/CNTs (inset shows size distribution). (E-G) HRTEM images of Pt_8Ag_4 clusters/CNTs [inset in (F) shows size distribution]. (H-J) Elemental maps of Pt and Ag in Pt_8Ag_4 cluster/CNT hybrids. PXRD: Powder X-ray diffraction; HRTEM: high-resolution transmission electron microscopy; MOC: metallic organic clusters; CNT: carbon nanotubes.

show the elemental mapping images of Ag and Pt for the Pt_8Ag_4 clusters/CNTs, suggesting that Pt and Ag are well overlapped in each cluster and are uniformly distributed on the CNTs, as further verified by the high-angle annular dark-field (HAADF) image. The inductively coupled plasma mass spectrometry measurements [Supplementary Table 2] reveal that the atomic ratio of Pt (3.86 wt.%) and Ag (0.896 wt.%) is close to 2:1, consistent with the atomic ratio in the MOCs.

Figure 2A and B show the HAADF-STEM images of the Pt_8Ag_4-clusters/CNTs, in which a number of nanoclusters are uniformly decorated on the CNT surface. The structure of the Pt_8Ag_4 clusters/CNTs was further studied by X-ray absorption near edge structure (XANES) and extended X-ray absorption fine structure (EXAFS), which are sensitive to electronic and local atomic structures. Figure 2C presents the XANES of the Pt L_3-edge for the Pt_8Ag_4 clusters/CNTs. The intensity of the white lines (main peak) in the XANES at the Pt L_3-edge derives from the 2p→5d transition and thus reflects the occupied electron information of the Pt 5d orbitals, which can be used to estimate the oxidation state of the Pt ions. The intensity of the main peak for the Pt L_3-edge absorption increases in the order of Pt_8Ag_4 MOCs/CNTs > Pt_8Ag_4 clusters/CNTs > Pt/CNTs > Pt foil [Figure 2C, Supplementary Figure 3A, and Supplementary Table 2], indicating that the average valence state of Pt_8Ag_4 MOCs/CNTs, Pt_8Ag_4 clusters/CNTs and Pt/CNTs is

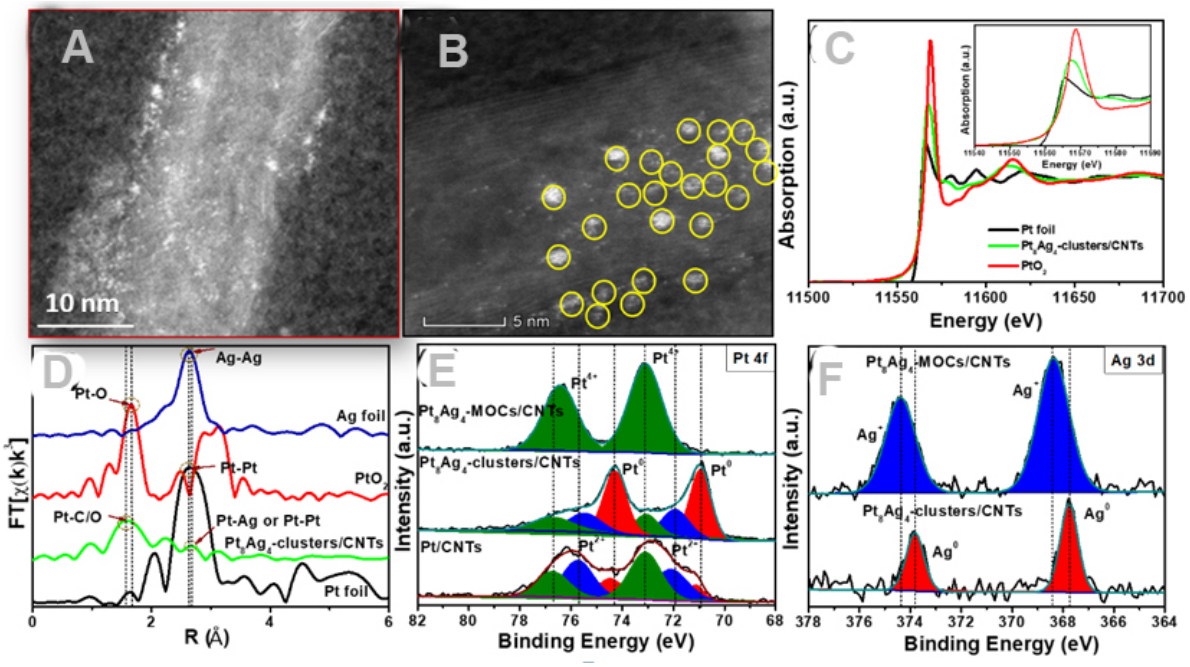

Figure 2. (A, B) HAADF-STEM images of Pt_8Ag_4 clusters/CNTs. (C) XANES and (D) EXAFS spectra of Pt_8Ag_4 clusters/CNTs, PtO_2 and Pt foil. (E) High-resolution XPS Pt 4f spectra and (F) Ag 3d spectra in Pt_8Ag_4 MOCs/CNTs and Pt_8Ag_4 clusters/CNTs. CNT: Carbon nanotubes; MOC: metallic organic clusters; XPS: X-ray photoelectron spectroscopy.

between zero and 4+[10].

The Pt EXAFS spectra of the Pt_8Ag_4 clusters/CNTs show a very weak peak at ~2.7 Å [Figure 2D, Supplementary Figure 3B], which is similar to the Pt-Pt shell peak in Pt foil (2.65 Å) and also close to the Pt-Ag shell peak in the PtAg alloy (2.64 Å). Furthermore, the apparent first shell peak at ~1.56 Å was ascribed to the Pt-C/O interaction, revealing that Pt in the Pt_8Ag_4 clusters/CNTs was formed as PtAg alloy nanoclusters. X-ray photoelectron spectroscopy (XPS) was also carried out to investigate the elemental composition and analyze the chemical state of the respective elements [Supplementary Figure 4]. Figure 2E shows the high-resolution XPS spectrum of Pt 4f, where the Pt_8Ag_4 MOCs/CNTs are quite similar to the form of Pt^{4+}. However, both the metallic and oxidation states (Pt^{2+} and Pt^{4+}) of Pt are present in the Pt_8Ag_4 clusters/CNTs. Although metallic Pt is the major phase in Pt_8Ag_4-cluster /CNTs, the major phases in Pt_8Ag_4 MOCs/CNTs and Pt/CNTs are the oxidation states (Pt^{2+} and Pt^{4+}) of Pt. The high-resolution XPS spectrum of Ag 3d is displayed in Figure 2F, which reveals that the Ag in the Pt_8Ag_4 clusters/CNTs is metallic Ag, different from that (Ag^+) in Pt_8Ag_4 MOCs/CNTs[27,28]. By combining the results of the elemental maps, EXAFS spectra and XPS data, it can be found that the PtAg alloy bonded with the MOC or CNT substrates after electrochemical reduction[29].

The electrocatalytic properties of the Pt_8Ag_4 clusters/CNTs for the HER were evaluated using linear sweep voltammetry (LSV) at room temperature in 0.5 M H_2SO_4. A set of electrodes, including PtMLs/CNTs, Pt/CNTs, Pt_8Ag_4 MOCs/CNTs, Pt_8Ag_4 MOCs, Pt_8Ag_4 clusters and the commercial Pt/C, were prepared as references for comparison. Figure 3A and Supplementary Figure 5 show the LSV curves of the set of electrodes. The overpotential at 10 mA cm^{-2} (η_{10}) for the Pt_8Ag_4 clusters/CNTs is 18 mV, which is much lower than those of PtMLs/CNTs (408 mV), Pt/CNTs (117 mV), Pt_8Ag_4 MOCs/CNTs (101 mV), Pt_8Ag_4 MOCs (217 mV), Pt_8Ag_4 clusters (78 mV) and Pt/C (77 mV) [Figure 3B-C, Supplementary Table 3].

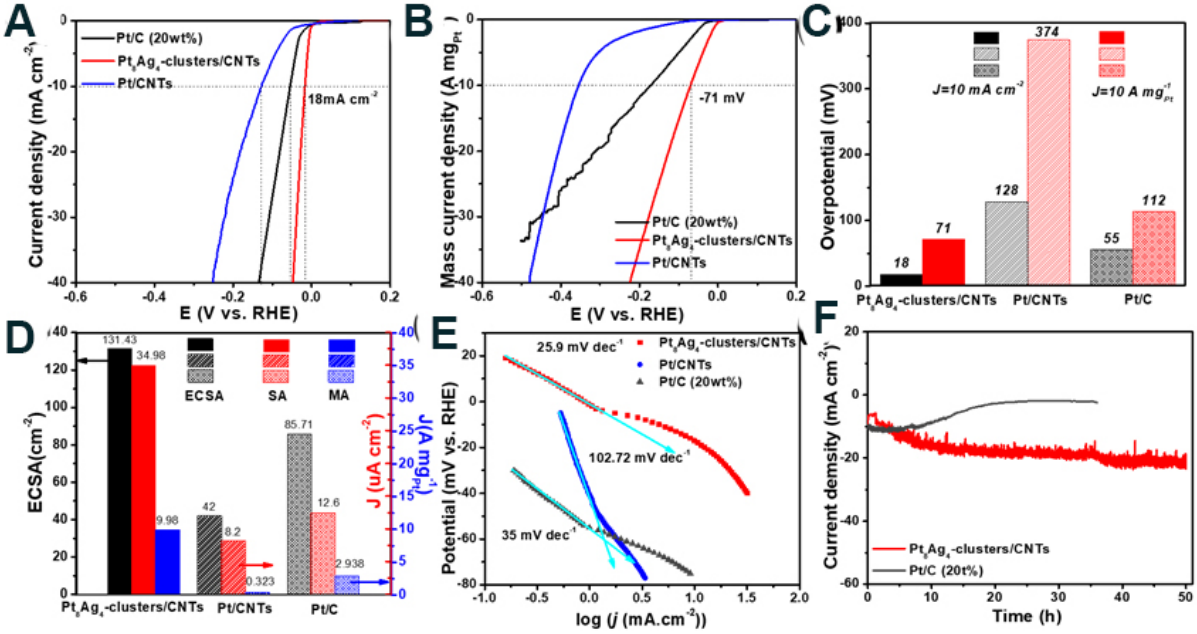

Figure 3. LSV curves of different electrodes based on (A) geometric area of electrode and (B) Pt mass loading in 0.5 M H2SO4 at a scan rate of 5 mV s-1. (C) Bar diagram for η10 at different electrodes. (D)Comparison of ECSA (left axis), current density normalized SA (right axis) and MAs (normalized by Pt mass, right axis) for HER at -70 mV for different electrodes. (E) Tafel slope for HER catalysis at different electrodes. (F) Chronopotentiometric measurements of long-term stability at -0.23 V. LSV: Linear sweep voltammetry; ECSA: electrochemical surface area; HER: hydrogen evolution reaction.

Furthermore, the LSV curves are normalized by net Pt mass [Figure 3B]. The mass activity at -70 mV for the Pt_8Ag_4 clusters/CNTs reaches as high as 9.98 A mg_{Pt}^{-1}, which is 50 times higher than that of the Pt/CNTs (0.32 A mg_{Pt}^{-1}) and three times higher than that of the commercial Pt/C (2.94 A mg_{Pt}^{-1}). These results signify that the alloyed Pt_8Ag_4 cluster contributes to the significantly enhanced mass activity for the HER.

Cycling within a non-Faradaic region at various scan rates allow us to calculate the double-layer capacitance (C_{dl}), which is 4.60, 1.47 and 3.04 mF cm^{-2} for Pt_8Ag_4 clusters/CNTs, Pt/CNTs and Pt/C, respectively [Supplementary Figure 6, Supplementary Table 4]. The electrochemical surface area (ECSA) [Figure 3D]evaluated based on C_{dl} was ~131.43 cm^2 for the Pt_8Ag_4 clusters/CNTs, which is three times larger than that (38.57 cm^2) for the Pt/CNTs, suggesting that atomistically Ag-engineered Pt also leads to an increase in activity sites. The current densities of different electrodes are thus normalized to the ECSA, which can provide information to evaluate the intrinsic activity. The Pt_8Ag_4 clusters/CNTs exhibit a current density of 35.0 μA cm^{-2} at -70 mV, at least 2.5 times higher than those of both Pt/CNTs (8.2 μA cm^{-2}) and Pt/C (12.6 μA cm^{-2}), demonstrating that the Pt_8Ag_4 clusters hold a much higher intrinsic catalytic activity for the HER. The specific current densities for the other electrodes, *i.e.*, Pt_8Ag_4 MOCs/CNTs, Pt_8Ag_4 MOCs and PtMLs/CNTs, are remarkably lower than for their electrochemically reduced electrode counterparts [Supplementary Figure 5], further signifying that the electrochemical reduction treatment can significantly boost the associated intrinsic activity. It is noteworthy that there is only a slight difference in the specific current density between the Pt_8Ag_4 clusters/CNTs and Pt_8Ag_4 clusters, implying that the CNT support in the hybrids significantly contributes to the increased number of active sites, other than the intrinsic activity.

Tafel plots were constructed to study the reaction kinetics and the HER mechanism [Figure 3E]. The slope of 25.9 mV dec^{-1} for the Pt_8Ag_4 clusters/CNTs suggests that the Tafel step ($H_{ads} + H_{ads} \rightarrow H_2$) is the rate-determining step[30-32]. The Tafel slopes of the set of catalysts decrease in the following order: Pt_8Ag_4

clusters/CNTs < Pt/C < Pt_8Ag_4 clusters < Pt_8Ag_4 MOCs/CNTs < Pt/CNTs < Pt_8Ag_4 MOCs < PtMLs/CNTs, verifying that the Pt_8Ag_4 clusters/CNTs have the highest catalytic kinetics toward the HER. In addition, electrochemical impedance spectroscopy signifies the lowest charge transfer resistance of the Pt_8Ag_4 clusters/CNTs among all the electrodes [Supplementary Figure 7, Supplementary Table 5], indicating the improved electron transfer rate upon catalysis of the HER. The chronoamperometric test [Figure 3F] on the Pt_8Ag_4 cluster/CNT electrodes was conducted by applying an overpotential of 33 mV (*vs.* RHE), which shows the capability of running for over 50 h with a gradual increase in current density. In contrast, the Pt/C electrode at an overpotential of 75 mV displayed a rather rapid drop in current density within 10 h.

We also investigated the HER catalytic performance of the Pt_8Ag_4 clusters/CNTs in alkaline (1 M KOH, pH 14) and neutral (1 M, PBS, pH 7) solutions. As expected, the Pt_8Ag_4 clusters/CNTs exhibit the highest catalytic activity toward the HER of all the samples, requiring a lower overpotential to reach the current density of 10 mA cm^{-2} and showing a smaller Tafel slope than that in the commercial Pt/C [Supplementary Figure 8, Supplementary Table 6-7]. In addition, the catalytic properties toward the oxygen reduction reaction (ORR) were also studied on these catalysts using the rotating disc electrode technique in 0.5 M H_2SO_4 and 1.0 M KOH. As shown in Supplementary Figure 9-11, the Pt_8Ag_4 clusters/CNTs show onset potentials (E_{onset}) of 0.906 and 0.966 V in 0.5 M H_2SO_4 and 1.0 M KOH, respectively. These values are more positive than those of the Pt/CNTs and Pt/C [Supplementary Table 8 and 9], suggesting a more pronounced ORR electrocatalytic activity for the Pt_8Ag_4 clusters/CNTs than the Pt/CNTs and the commercial Pt/C.

Density functional theory (DFT) calculations were employed to acquire atomic insights into the HER activity of the Pt_8Ag_4/CNT catalysts. The model structure of the Pt_8Ag_4 clusters/CNTs is shown in Figure 4A and the reference Pt/CNTs are shown in Supplementary Figure 12. The value of ΔE_{H^*} (Gibbs energy of absorption of H*) is introduced as an effective activity descriptor for the HER activity and a catalyst with $\Delta E_{H^*} = 0$ can be considered as an outstanding candidate for the HER. Therefore, the adsorption free energy of H (ΔE_{H^*}) at different sites (Supplementary Figure 13 and 14) on the Pt_8Ag_4 clusters/CNTs and Pt/CNTs was calculated to evaluate their HER activity. The results suggest that the Pt site of the Pt_8Ag_4/CNTs has excellent activity for the HER. As shown in Figure 4B, the ΔE_{H^*} at dominant active sites in the Pt_8Ag_4 clusters/CNTs is close to the ideal value of the HER, which proves that the introduction of Ag atoms to Pt_8Ag_4/CNTs contribute to the improved HER activity. In contrast, the Pt_8Ag_4/CNTs also have superior performance for the ORR. The value of ΔE_{O^*} (Gibbs energy of adsorption of O*) is used to assess the ORR activity of catalysts based on the theoretical volcano relationship[33]. The positions of oxygen atoms adsorbed on the cluster were found by DFT calculations, as shown in Supplementary Figure15. As shown in Figure 4C, the ORR activity of the Pt_8Ag_4 clusters/CNTs is higher than that of the Pt/CNTs based on the theoretical volcano model, which is also consistent with the experimental results. Therefore, the introduction of Ag to the Pt_8Ag_4-clusters/CNTs leads to high activity toward both ORR and HER catalysis.

CONCLUSION

In summary, we here presented a new CNT-supported alloyed nanocluster hybrid catalyst derived from a unique bimetallic organic cluster, which shows remarkably boosted catalytic activity with an ultralow Pt content loading. This study provides a new synthetic method for a bimetallic alloy cluster with an elaborately designed supramolecular precursor, dedicating to the high density of atomically controlled active sites to promote the associated mass catalytic activity. The present work may open a promising strategy for the controllable synthesis of advanced catalysts for a variety of electrochemical applications.

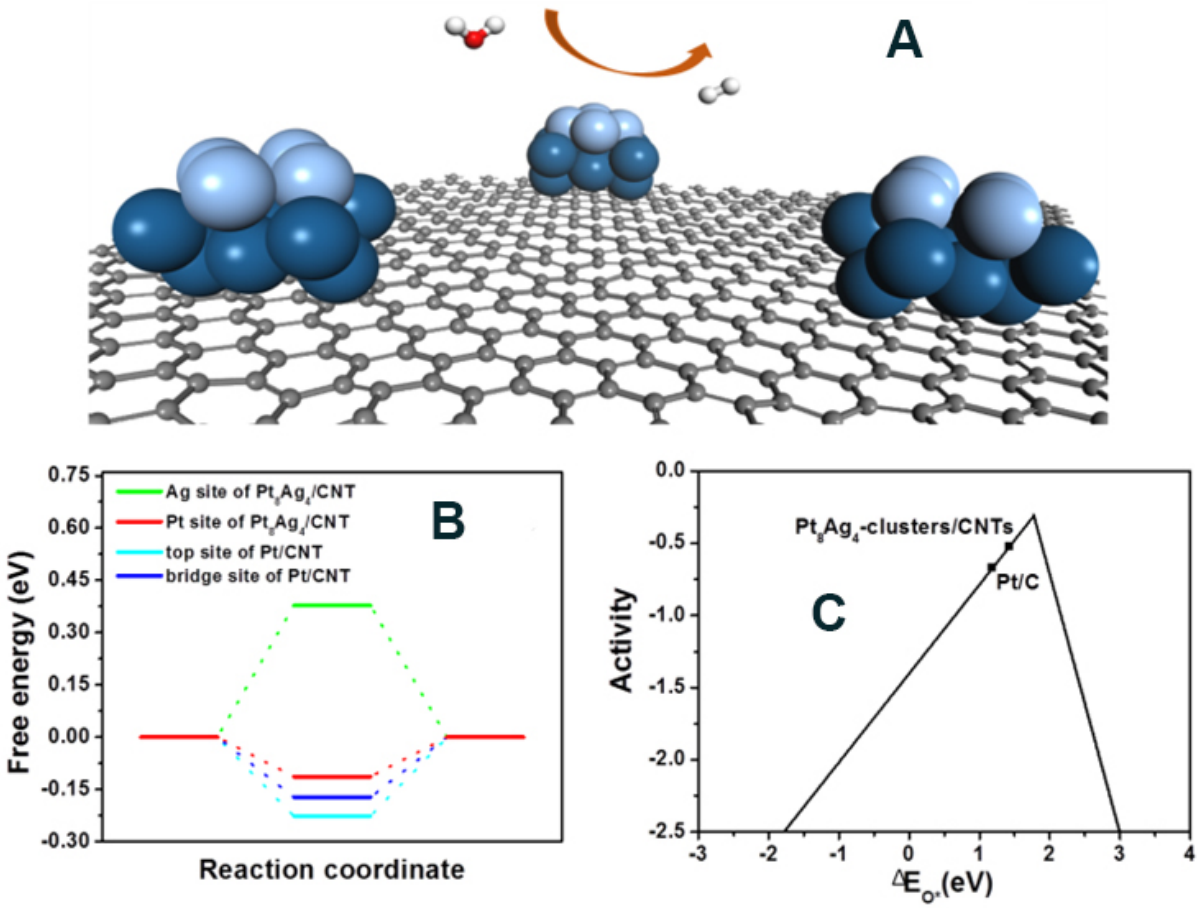

Figure 4. DFT calculation results. (A) Structure diagram of Pt_8Ag_4 clusters on CNTs. (Dark blue, light blue, grey, red and white atoms represent Pt, Ag, C, O and H, respectively.) (B) Free energy profiles for hydrogen adsorption at different active sites of Pt_8Ag_4 clusters/CNTs and Pt/CNTs. (C) ORR activities of Pt_8Ag_4 clusters/CNTs and Pt/CNTs predicted by the calculated oxygen adsorption energy ($\triangle E_{O^*}$) based on the theoretical volcano relationship. DFT: Density functional theory; CNT: carbon nanotubes; ORR: oxygen reduction reaction.

DECLARATIONS

Acknowledgments

Authors would like to acknowledge 1W1B station of BSRF and BL14W1 station of SSRF for synchrotron beam time.

Authors' contributions

Liangzhen Liu and Qiang-Yu Zhu contribute equally to this work

Made substantial contributions to conception and design of the study and performed data analysis and interpretation: Liangzhen Liu, Qiang-Yu Zhu, Junheng Huang, Zhenhai Wen, Qing-Fu Sun

DFT calculation: Junwei Li, Junxiang Chen

Availability of data and materials

Not applicable.

Financial support and sponsorship

This work was supported by the National Natural Science Foundation of China (Grant Nos. 21875253, 21701175 and 21703248)

Conflicts of interest

All authors declare that they are bound by confidentiality agreements that prevent them from disclosing their conflicts of interest in this work.

Ethical approval and consent to participate

Not applicable.

Consent for publication

Not applicable.

REFERENCES

1. Desireddy A, Conn BE, Guo J, et al. Ultrastable silver nanoparticles. *Nature* 2013;501:399-402. DOI PubMed
2. Negreiros FR, Halder A, Yin C, et al. Bimetallic Ag-Pt sub-nanometer supported clusters as highly efficient and robust oxidation catalysts. *Angew Chem Int Ed Engl* 2018;57:1209-13. DOI PubMed
3. Gong Y N, Jiao L, Qin Y, et al. Regulating the coordination environment of MOF-templated single-atom nickel electrocatalysts for boosting CO2 reduction. Angewandte Chemie 2020;132:2727-31. DOI PubMed
4. Fang X, Shang Q, Wang Y, et al. Single Pt atoms confined into a metal-organic framework for efficient photocatalysis. *Adv Mater* 2018;30:1705112. DOI PubMed
5. Kratzl K, Kratky T, Günther S, et al. Generation and stabilization of small platinum clusters $Pt_{12\pm x}$;141:13962-9. DOI PubMed
6. Imaoka T, Kitazawa H, Chun WJ, Yamamoto K. Finding the most catalytically active platinum clusters with low atomicity. *Angew Chem Int Ed Engl* 2015;54:9810-5. DOI PubMed
7. Bai S, Bu L, Shao Q, et al. Multicomponent Pt-based zigzag nanowires as selectivity controllers for selective hydrogenation reactions. J Am Chem Soc 2018;140:8384-87. DOI PubMed
8. Bu L, Zhang N, Guo S, et al. Biaxially strained PtPb/Pt core/shell nanoplate boosts oxygen reduction catalysis. *Science* 2016;354:1410-4. DOI PubMed
9. Li Q, Wen X, Wu G, Chung HT, Gao R, Zelenay P. High-activity PtRuPd/C catalyst for direct dimethyl ether fuel cells. *Angew Chem Int Ed Engl* 2015;54:7524-8. DOI PubMed
10. Li M, Duanmu K, Wan C, et al. Single-atom tailoring of platinum nanocatalysts for high-performance multifunctional electrocatalysis. *Nature Catalysis* 2019;2:495-503. DOI
11. Liang J, Li N, Zhao Z, et al. Tungsten-Doped $L1_0$-PtCo ultrasmall nanoparticles as a high-performance fuel cell cathode. *Angew Chem Int Ed Engl* 2019;58:15471-7. DOI PubMed
12. Sun M, Ji J, Hu M, et al. Overwhelming the performance of single atoms with atomic clusters for platinum-catalyzed hydrogen evolution. *ACS Catalysis* 2019;9:8213-23. DOI
13. Zhang B, Sun G, Ding S, et al. Atomically dispersed Pt_1-polyoxometalate catalysts: how does metal-support interaction affect stability and hydrogenation activity? *J Am Chem Soc* 2019;141:8185-97. DOI PubMed
14. Zhang J, Zhao Y, Guo X, et al. Single platinum atoms immobilized on an MXene as an efficient catalyst for the hydrogen evolution reaction. *Nat Catal* 2018;1:985-92. DOI
15. Bai L, Wang X, Chen Q, et al. Explaining the size dependence in platinum-nanoparticle-catalyzed hydrogenation reactions. *Angew Chem Int Ed Engl* 2016;55:15656-61. DOI PubMed
16. Liu P, Zhao Y, Qin R, et al. Photochemical route for synthesizing atomically dispersed palladium catalysts. *Science* 2016;352:797-801. DOI PubMed
17. Lang R, Li T, Matsumura D, et al. Hydroformylation of olefins by a rhodium single-atom catalyst with activity comparable to $RhCl(PPh_3)_3$. *Angew Chem Int Ed Engl* 2016;55:16054-8. DOI PubMed
18. Zhao Y, Jiang WJ, Zhang J, et al. Anchoring sites engineering in single-atom catalysts for highly efficient electrochemical energy conversion reactions. *Adv Mater* 2021;33:e2102801. DOI PubMed
19. Ji S, Chen Y, Fu Q, et al. Confined pyrolysis within metal-organic frameworks to form uniform Ru_3 clusters for efficient oxidation of alcohols. *J Am Chem Soc* 2017;139:9795-8. DOI PubMed
20. Liu H, Chang L, Bai C, Chen L, Luque R, Li Y. Controllable encapsulation of “Clean” metal clusters within MOFs through kinetic

modulation: towards advanced heterogeneous nanocatalysts. *Angew Chem* 2016;128:5103-7. DOI PubMed PMC

21. Feng Y-Y, Ma J-H, Zhang G-R, et al. Dealloyed carbon-supported PtAg nanostructures: enhanced electrocatalytic activity for oxygen reduction reaction. *Electrochemistry communications* 2010;12:1191-94. DOI
22. Zhang J, Zhao Y, Chen C, et al. Tuning the coordination environment in single-atom catalysts to achieve highly efficient oxygen reduction reactions. *J Am Chem Soc* 2019;141:20118-26. DOI PubMed
23. Zhao Y, Zhang J, Xie Y, et al. Constructing atomic heterometallic sites in ultrathin nickel-incorporated cobalt phosphide nanosheets via a boron-assisted strategy for Highly efficient water splitting. *Nano Lett* 2021;21:823-32. DOI PubMed
24. Yu S, Lou Q, Han K, et al. Synthesis and electrocatalytic performance of MWCNT-supported Ag@ Pt core-shell nanoparticles for ORR. *International journal of hydrogen energy* 2012;37:13365-70. DOI
25. Zheng F, Luk S, Kwong T, Yung K. Synthesis of hollow PtAg alloy nanospheres with excellent electrocatalytic performances towards methanol and formic acid oxidations. *RSC Adv* 2016;6:44902-7. DOI
26. Liu L, Ci S, Bi L, Jia J, Wen Z. Three-dimensional nanoarchitectures of Co nanoparticles inlayed on N-doped macroporous carbon as bifunctional electrocatalysts for glucose fuel cells. *J Mater Chem A* 2017;5:14763-74. DOI
27. Liu Y, Kong J, Yuan J, et al. Enhanced photocatalytic activity over flower-like sphere Ag/Ag2CO3/BiVO4 plasmonic heterojunction photocatalyst for tetracycline degradation. *Chemical Engineering Journal* 2018;331:242-54. DOI
28. Zhu Q, Wang W, Lin L, et al. Facile synthesis of the novel Ag_3VO_4/AgBr/Ag plasmonic photocatalyst with enhanced photocatalytic activity and stability. *J Phys Chem C* 2013;117:5894-900. DOI
29. Zhao Z, Liu H, Gao W, et al. Surface-engineered PtNi-O nanostructure with record-high performance for electrocatalytic hydrogen evolution reaction. *J Am Chem Soc* 2018;140:9046-50. DOI PubMed
30. Wang J, Xu F, Jin H, Chen Y, Wang Y. Non-noble metal-based carbon composites in hydrogen evolution reaction: fundamentals to applications. *Adv Mater* 2017:29. DOI PubMed
31. Fletcher S. Tafel slopes from first principles. *Journal of Solid State Electrochemistry* 2009;13:537-49. DOI: 10.1007/s10008. DOI
32. Xu S, Kim Y, Park J, et al. Extending the limits of Pt/C catalysts with passivation-gas-incorporated atomic layer deposition. *Nat Catal* 2018;1:624-30. DOI
33. Nørskov JK, Rossmeisl J, Logadottir A, et al. Origin of the overpotential for oxygen reduction at a fuel-cell cathode. *J Phys Chem B* 2004;108:17886-92. DOI